Jones, T. A., and C. Nixon, 2017: Short-term forecasts of left-moving supercells from an experimental Warn-on-Forecast system. *J. Operational Meteor.*, **5** (13), 161-170, doi: https://doi.org/10.15191/nwajom.2017.0513

Short-term Forecasts of Left-Moving Supercells from an Experimental Warn-on-Forecast System

THOMAS A. JONES
Cooperative Institute for Mesoscale Meteorological Studies, University of Oklahoma, Norman, Oklahoma

CAMERON NIXON
Texas Tech University, Lubbock, Texas

(Manuscript received 10 March 2017; review completed 23 June 2017)

ABSTRACT

Most research in storm-scale numerical weather prediction has been focused on right-moving supercells as they typically lend themselves to all forms of high-impact weather, including tornadoes. As the dynamics behind splitting updrafts and storm motion have become better understood, differentiating between atmospheric conditions that encourage right- and left-moving supercells has become the subject of increasing study because of its implication for these weather forecasts. Despite still often producing large hail and damaging winds, left-moving (anticyclonically rotating in the Northern Hemisphere) supercells have received much less attention.

During the 2016, NOAA Hazardous Weather Testbed, the NSSL Experimental Warn-on-Forecast System for ensembles (NEWS-e) was run in real-time. One event in particular occurred on 8 May 2016 during which multiple left- and right- moving supercells developed in western Oklahoma and Kansas—producing many severe weather reports. The goal of this study was to analyze the near storm environment created by NEWS-e using wind shear and other severe weather parameters. Then, we sought to determine the ability of the NEWS-e system to forecast storm splits and the persistence of left- and right- moving supercells through qualitatively analyzing tracks of forecast updraft helicity. Initial results show that the NEWS-e system analyzed several areas favorable for left- and right-moving supercells during which the system forecasted storm splitting and the persistence of both storm types. In particular, hail-producing left-moving supercells were accurately forecast in central and northern Oklahoma while a tornado-producing right-moving supercell was forecast in southern Oklahoma.

1. Introduction

The basic theory of supercell storm splitting in an idealized environment is well understood. Given a straight-line hodograph representative of a unidirectionally sheared environment, substantial shear for supercells will ensure that both counterclockwise (cyclonic) and clockwise (anticyclonic) rotating updrafts are equally favored (e.g., Klemp and Wilhelmson 1978; Wilhelmson and Klemp 1978; Brown and Meitín 1994; Bunkers et al. 2000; Bunkers 2002). For typical upper-level wind patterns in the Northern Hemisphere, cyclonic (right moving) supercells are generally favored in any severe weather environment corresponding with a curved hodograph as winds tend to veer with height and strengthen especially in the lowest 3 km AGL (Davies-Jones 1985). However, in cases with more straight-line or even counterclockwise-turning hodographs, anticyclonic rotation (i.e., left-moving supercells) may become favored (Bunkers 2002; Fig. 1). Many instances of left-moving supercells have been documented over the years (e.g., Grasso and Hilgendorf 2001; Monteverdi et al. 2001; Bunkers 2002; Dostalek et al. 2004; Edwards et al. 2004; Edwards and Hodanish 2006; Smith et al. 2012), whose primary severe weather threats include large hail and damaging winds.

Corresponding author address: Dr. Thomas A. Jones, Cooperative Institute for Mesoscale Meteorological Studies, University of Oklahoma, and NOAA/OAR/National Severe Storms Laboratory, 120 David L. Boren Blvd., Norman, OK 73072
E-mail: Thomas.Jones@noaa.gov

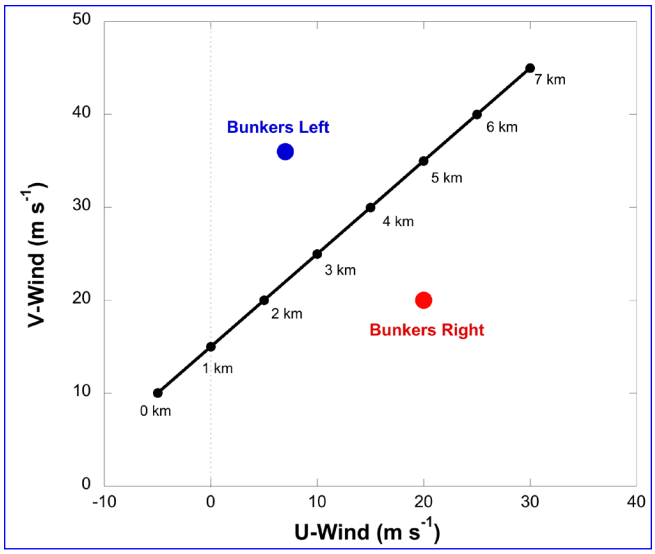

Figure 1. Idealized straight-line hodograph with Bunkers right- (red) and left- (blue) moving storm motions shown (using a 0–7-km mean wind). *Click image for an external version; this applies to all figures hereafter.*

However, tornadoes also have been shown to occur with left-moving supercells under ideal circumstances (e.g., Monteverdi et al. 2001).

This research assesses whether or not a Warn-on-Forecast (WoF) system (Stensrud et al. 2009, 2013)—such as the NSSL Experimental WoF System for ensembles (NEWS-e)—can accurately forecast the evolution of both left- and right-moving supercells within an environment favorable for severe weather that occurred on 8 May 2016. The specific goal of this study was to determine the ability of the NEWS-e system to predict these storms between 2130 and 0030 UTC using forecasts initiated at 2130 and 2300 UTC covering the period from near convective initiation to after when the storms became well established. Following the introduction, section 2 describes various severe weather parameters used in this study. Section 3 discusses the WoF data assimilation and forecasting system, and section 4 discusses the evolution of storms on 8 May 2016. Section 5 describes the near storm environment for selected analysis times, while section 6 discusses short-term (90 min) updraft helicity (UH) forecasts from these analyses. Conclusions are provided in section 7.

2. Severe weather parameters

Several analysis and forecasting parameters have been developed that can be used to determine if an environment is conducive for rotating, supercell storms. One such parameter, storm-relative helicity (SRH), is related to the potential for midlevel rotation through tilting and stretching of vorticity by a storm updraft (Davies-Jones et al. 1990; Brooks et al. 1994; Dostalek et al. 2004). Note that SRH can change in magnitude or sign owing to changes in the speed and direction of a storm's motion; thus, a storm motion to the left of the deep-layer shear vector typically implies that it ingests negative values of SRH. Low-level (0–1 km) SRH generally is positive because of (i) natural veering of the winds with height in warm-air advection regimes and (ii) strengthening of the wind with height as the impact of surface friction decreases. In cases where the veering ceases, SRH for the left-moving storm motion vector becomes negative, enabling deep-layer anticyclonic rotation to be sustained. The magnitudes of SRH suggesting "favorable" conditions for each direction of storm rotation may not be equal. In a sample of cyclonic and anticyclonic supercell environments, the median SRH for cyclonic supercells was 187 $m^2 s^{-2}$, while the median value for anticyclonic supercells was only –51 $m^2 s^{-2}$. To complicate matters, the median SRH was <150 $m^2 s^{-2}$ for >25% of right-moving supercells and positive for >25% of left-moving supercells (Bunkers 2002).

In addition to SRH, the supercell composite parameter (SCP) was created to further assess supercell-supportive conditions (Thompson et al. 2003, 2004b). SCP represents a combination of convective available potential energy (CAPE), effective SRH (ESRH), and effective bulk wind difference (EBWD) over the lower half of the expected storm depth. When combined, these variables form a unitless parameter that measures the favorability of the environment for the formation and sustainability of left- and right-moving supercells. Values of SCP generally range between –20 and 20, with positive values being associated with right-moving supercells and negative values associated with left-moving supercells.

UH is used as a proxy for tracking potential supercells in convection-permitting model output. It is calculated here using the ensemble mean layer-averaged relative vertical vorticity from the model levels between approximately 2 and 5 km and then multiplied by the individual layer depth (Kain et al. 2008). This output has become increasingly utilized in storm-scale forecasting; however, UH is generally displayed in the form of maximum or positive-only values, characteristic of standard cyclonically rotating,

right-moving supercell storms. The same method also works for anticyclonic rotation, but UH values become negative instead of positive. Thus, the magnitude of negative UH can be used to track anticyclonic rotation in much the same manner as it is currently used for cyclonically rotating storms.

3. Warn-on-Forecast system

This research uses the ensemble data assimilation system—described in detail by Wheatley et al. (2015) and Jones et al. (2016)—known as the NSSL experimental WoF System for ensembles (NEWS-e). The NEWS-e uses the Advanced Weather Research and Forecasting model (WRF-ARW) version 3.6.1 (Skamarock et al. 2008), coupled with the parallel ensemble adjustment Kalman filter in the Data Assimilation Research Testbed (Anderson and Collins 2007; Anderson et al. 2009), to assimilate observations at 15-min intervals in a 36-member ensemble. Initial and boundary conditions are provided by an experimental 20-member ensemble High Resolution Rapid Refresh (HRRR-e) model. The HRRR-e is an extension of the operational HRRR model, which is an hourly cycled, 3-km convection permitting model that generates 18-h forecasts from each analysis time (Benjamin et al. 2016). The NEWS-e system was initialized at 1800 UTC each day using 3-h forecasts generated from the first 18 members of the HRRR-e. The NEWS-e system also is run at 3-km grid spacing, but over a smaller domain so that 15-min cycling was possible with available computing resources. Both the HRRR-e and NEWS-e systems have 51 vertical levels extending from the surface to 10 hPa. Different sets of WRF model physics options are applied to each ensemble member to introduce the required model spread (e.g., Stensrud et al. 2000). All members use the Thompson cloud microphysics (Thompson et al. 2004a, 2008); no cumulus parameterization is applied on the storm-scale grid (Wheatley et al. 2015). The NEWS-e system assimilates Weather Surveillance Radar-1988 Doppler radial velocity and reflectivity observations, Geostationary Operational Environmental Satellite (GOES)-13 satellite cloud water path (CWP) retrievals (Jones et al. 2015), and Oklahoma mesonet data. All available observations are assimilated at 15-min intervals continuously from 1800 until 0300 UTC the next day. For the 8 May event, emphasis is placed on the analysis and forecasts generated between 2130 and 0030 UTC covering the time during which convection initiated, supercell storms split, and most of the severe weather reports occurred. Forecast output is generated at 5-min intervals over the duration of the forecast period. Additional details concerning the NEWS-e system (including localization radii, additive noise, adaptive inflation, observation errors, and model physics) can be found in Wheatley et al. (2015) and Jones et al. (2016). This system was successfully tested in real-time operations as part of the 2016 Hazardous Weather Testbed during May 2016, including the 8 May event discussed here (e.g., Jirak et al. 2014).

4. Observed storm evolution on 8 May 2016

To assess the ability of numerical weather prediction systems to forecast left-moving supercells, an event is required where the synoptic and mesoscale environment are favorable for their occurrence and appropriate data are available to analyze the developing convection. These conditions were met for an event on 8 May 2016 when several supercells developed along a dryline in western Oklahoma and Kansas in response to an incoming upper-level trough coupled with surface based CAPE (SBCAPE) in excess of 3000 J kg^{-1}. The first storm complexes (A, B) developed in far southwestern Oklahoma by 2130 UTC (Fig. 2a), with additional development extending farther north by 2200 UTC that generated storm complexes C and D. (Fig. 2b). By 2230 UTC, the southernmost cluster gave rise to a long-lived right-moving supercell (A1) that generated the sole tornado report associated with this event along with a swath of damaging wind (Fig. 2c). The corresponding left-moving supercell (A2) generated several reports of severe hail [diameter ≥1.0 in (2.5 cm)], including one significant hail report [diameter ≥2 in (5.1 cm); Fig. 2b,c; Table 1]. At 2300 UTC, another left-moving supercell, A3, split off A1 and proceeded to generate additional hail reports during the next hour (Fig. 2d).

Out of the B complex, a storm split resulted in a right-moving supercell (B1) that quickly dissipated; however, a long-lived left-moving supercell (B2) eventually produced severe hail up to 7.0 cm (2.75 in) in diameter (Fig. 2b–e; Table 1). Along the Oklahoma/Kansas border, a long-lived right- and left-moving pair formed (C1, C2), with both producing severe hail (Fig. 2c–f). The right-moving supercell (C1) eventually merged with the long-lived left-moving supercell (B2) in north-central Oklahoma (Fig. 2f), and both dissipated shortly thereafter. Slightly farther north, one more right- and left-moving pair developed (D1 and D2), with the right-moving supercell (D1) merging into the left-moving supercell (C2) that was coming up from

Table 1. Severe weather reports associated with each storm complex between 2000 and 0100 UTC 8 May 2016. Significant (Sig) hail is defined as hail with a diameter ≥5.1 cm (2 in) and significant wind is defined as straight-line wind ≥33.4 m s^{-1} (65 kt).

STORM	Type	Tornado	Hail (Sig)	Wind (Sig)
A1	Right	1	1	5
A2	Left	0	4 (1)	0
A3	Left	0	3	0
B1	Right	0	0	0
B2	Left	0	2 (1)	0
C1	Right	0	1	0
C2	Left	0	1	0
D1	Right	0	0	0
D2	Left	0	2 (1)	0
E1	Right	0	1	0
E2	Left	0	2	0

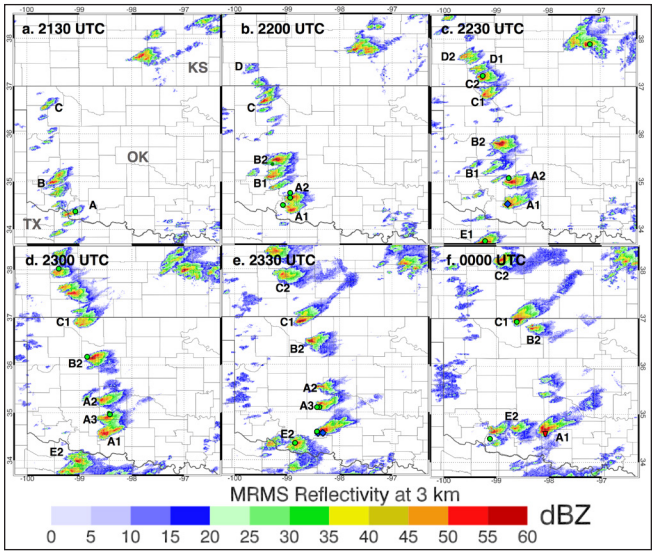

Figure 2. Multi-radar multi-sensor (MRMS) 3-km AGL reflectivity analyses at 2130 (a), 2200 (b), 2230 (c), 2300 (d), 2330 (e), and 0000 (d) UTC 8–9 May 2016. Letters denote individual storm complexes with A1, B1, C1, D1, and E1 being right-moving supercells and A2, A3, B2, C2, D2, and E2 being left-moving supercells. Severe storm reports (green = hail, blue = wind, and red = tornado) within ±15 min of each analysis time are overlaid.

the Oklahoma/Kansas border, while the left-moving supercell (D2) produced significant severe hail up to 7.6 cm (3 in) in diameter (Fig. 2c,d; Table 1). Finally, an additional splitting storm complex (E1, E2) moved into the southwestern portion of the domain after 2230 UTC (Fig. 2c–f). The left-moving supercell (E2) generated ≥2 diameter hail reports in southern Oklahoma before weakening after 0000 UTC. Note that left-moving supercells accounted for all three significant hail reports and >50% the total hail reports (Table 1).

5. Environmental analysis

a. 2130 UTC

The favorability of the modeled environment towards left- and right-moving supercells can be determined by analyzing the wind-shear characteristics generated by the model. Recall that convection developed by 2130 UTC in western and southwestern Oklahoma, representing the precursors to storm complexes A, B, and C (Fig. 2a). Splitting of the developing convection into left- and right-moving supercells occurred over the next hour (Fig. 2c). Each storm moved into a unique environment that was supportive of either or both storm types.

Figure 3 shows the ensemble mean 0–3- and 0–1-km SRH and left-moving SRH (LSRH) for left- and right-moving supercells, respectively, at 2130 UTC 8 May over western Oklahoma and southern Kansas. Cyclonic (or right moving) SRH is calculated assuming a Bunkers storm motion of 7.5° right of the mean 0–6-km shear vector through the 0–6-km mean wind. LSRH is similar, but uses a storm motion 7.5° left of the mean shear vector. The model results show that the 0–3-km SRH is ≥100 m^2 s^{-2} over much of western Oklahoma and southern Kansas, with a band of >250 m^2 s^{-2} located in southern Oklahoma (Fig. 3a). Thus, the entire region is moderately favorable for right-moving supercells, with the area in southern Oklahoma being the most favorable. The corresponding LSRH differs in that the absolute maximum (i.e., most negative) values are located in central Oklahoma and northward, with much

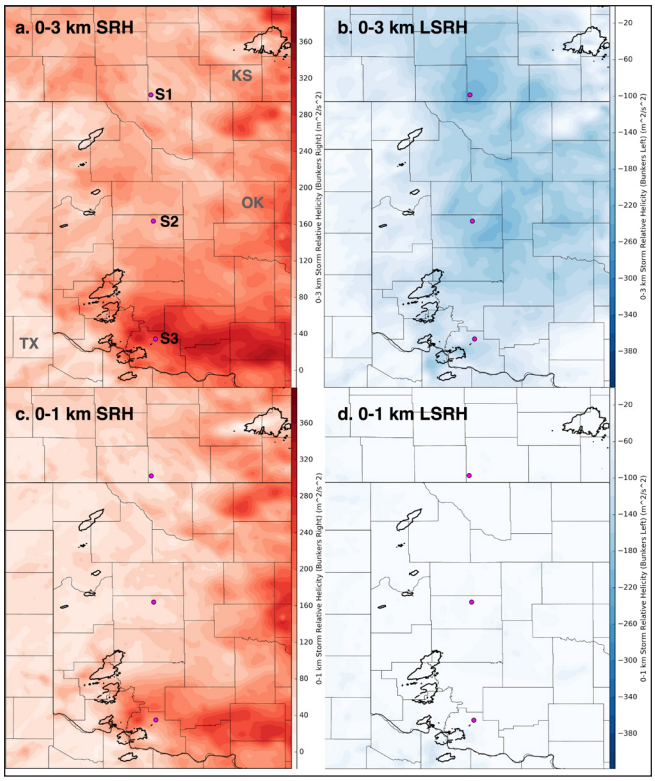

Figure 3. Ensemble mean 0–3-km (a,b) and 0–1-km (c,d) storm-relative helicity (SRH, left column) and left-moving SRH (LSRH, right column) at 2130 UTC. MRMS 3-km AGL reflectivity >25 dBZ is overlaid with black lines. Pink dots (S1, S2, S3) indicate locations of hodographs shown in Fig. 4a–c.

lower values in southern Oklahoma (Fig. 3b). Thus, long-lived left-moving supercells are possible in the northern half of the domain.

To further understand the wind shear characteristics in various parts of the domain, hodographs and corresponding severe weather parameters were generated from the ensemble mean analysis at 2130 UTC for three locations (S1, S2, and S3; Fig. 4). These locations were selected to represent the near storm environment of storm complexes C/D, B, and A, respectively. Overall, the wind shear environment throughout western Oklahoma appears supportive of left-moving supercells with LSRH often ≤100 m^2 s^{-2} when assuming the Bunkers storm motions. At the northernmost location (S1), the overall wind profile above 1 km favors left-moving supercells with an LSRH of –211 m^2 s^{-2}, compared to an SRH of only 75 m^2 s^{-2} (Fig. 4a, Table 2). However, the 0–1-km wind profile remains weakly favorable for cyclonic rotation with an SRH of 38 m^2 s^{-2}, but with an LSRH of 0. Based on the wind shear at this location, left-moving supercells would be favored over their right-moving counterparts. However, the analyzed conditions still indicate the possibility of severe weather-producing right-moving supercells in this region.

Farther south in central Oklahoma at location S2, the environment remains favorable for left-moving supercells, but also is increasingly favorable for right-moving supercells with 0–3-km LSRH and SRH being –165 and 109 m^2 s^{-2}, respectively (Fig 4c, Table 2). Also, the 0–1-km wind shear is similar to that at location S1, being weakly favorable for cyclonic rotation. The southernmost location at S3 is located in the environment much more favorable for right-moving supercells. The change in hodograph curvature because of the stronger southwesterly ground-relative winds

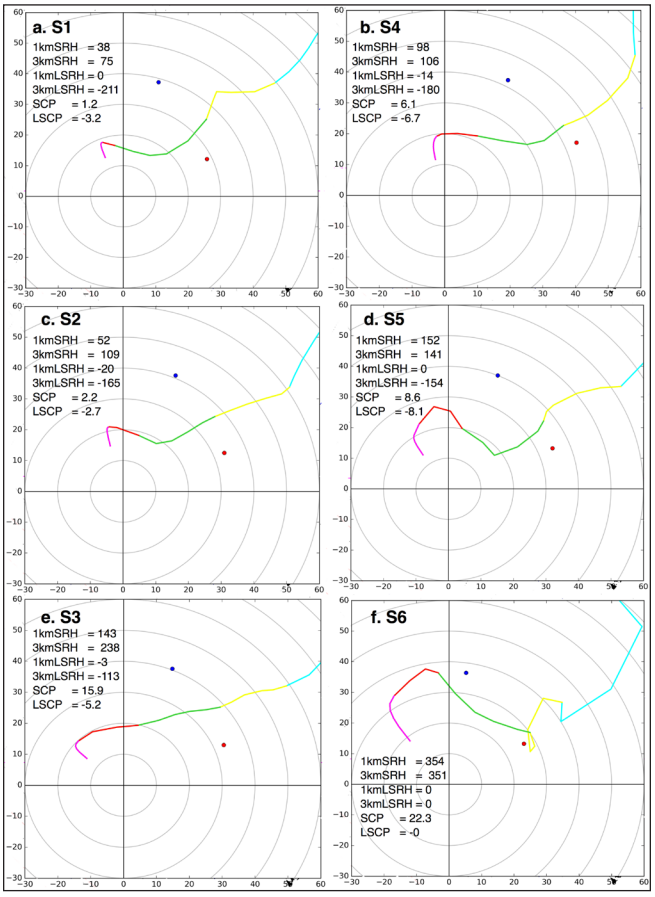

Figure 4. Ensemble mean hodographs at 2130 UTC for locations S1 (a), S2 (c), and S3 (e) and 2300 UTC for locations S4 (b), S5 (d), and S6 (f). Colors indicate height above surface: pink (0–500 m), red (500–1000 m), green (1–3-km), yellow (3–6-km), and cyan (6–12-km). Red and blue dots represent right- and left-moving Bunkers storm motions, respectively.

at S3 compared to the S1 and S2 locations reduces LSRH and increases SRH at these levels (Fig. 4e). Also, 0–1-km SRH is larger (143 m^2 s^{-2}), indicating a greater favorability of tornado-producing, right-moving supercells. The corresponding 0–1-km LSRH is very small. Overall, the wind shear environment is most supportive of left-moving supercells in northern Oklahoma, while stronger, right-moving supercells are more likely to occur and persist in far southern Oklahoma.

Finally, it also is necessary to consider thermodynamic conditions in these regions to determine whether or not convection is likely to develop and persist in regions otherwise favorable for left- and right-moving supercells. At all profile locations, SBCAPE exceeds 3000 J kg^{-1} with little convective inhibition (CIN), indicating an atmosphere primed for the severe convection (Table 2). Figure 5a shows SCP, which combines wind-shear and instability parameters into a single variable that represents the favorability of the atmosphere for right-moving supercells. At 2130 UTC, the ensemble mean SCP is maximized in southern Oklahoma with values in excess of 15 (Fig. 5a). Farther north, SCP is much smaller in the vicinity of developing storm complexes B and C. For anticyclonic, or left-moving SCP (LSCP), negative values indicate an environment conducive for left-moving supercells. The highest absolute values of LSCP are located in a small region in southwestern Oklahoma, with local maximums that are likely enhanced by convective cold pools and/or subtle storm boundaries that may be less representative of the overall environment (Fig. 5b). Larger areas of negative LSCP are present in a zonal band along the dryline just north of the area of highest SCP, with another region of enhanced negative LSCP present in far northern Oklahoma and southern Kansas.

b. 2300 UTC

Several changes to the environment occur by 2300 UTC that impact the evolution of the convection. Both 0–3- and 0–1-km SRH increase over most of the domain compared to 2130 UTC, indicating additional favorability towards right-moving supercells (Fig. 6a,c). The greatest SRH is again located in southern Oklahoma near and ahead of storm complex A while LSRH has decreased in most areas (Fig. 6b,d). Some areas of high LSRH remain, especially to the northeast of left-moving supercells A2, A3, and B2. This is evident from analyzing ensemble mean hodographs at locations S4 and S5 (Fig. 4b, d). Location S4 represents the near storm environment associated with B2 with an LSRH of –180 m^2 s^{-2}, but only an SRH of 106 m^2 s^{-2}. As before, the 0–1-km wind shear favors cyclonic rotation while the 1–3-km shear is more favorable for anticyclonic rotation (Fig. 4b). A similar pattern exists in the environment around storms A2 and A3, which is shown by the hodograph at S5 (Fig. 4d). Here, the 0–1-km wind shear is much more pronounced with an SRH value of 152 m^2 s^{-2} (Table 2). Above 1 km, shear becomes favorable for anticyclonic rotation again with LSRH of –154 m^2 s^{-2} whereas SRH is only 141 m^2 s^{-2}. Both A2 and A3 form and persist in this environment. The locations of S4 and S5 are close enough to the storms that the analyzed LSRH may be increased over the background value owing to an increase in the surface wind speeds from storm inflow. The most favorable environment for cyclonic supercells remains in southern Oklahoma, with location S6 placed east of the tornado-producing right-moving supercell (A1, Fig. 4f). The hodograph shows an environment much more favorable for low-level cyclonic rotation in the lowest 1 km of the atmosphere. Both 0–1- and 0–3-km SRH exceed 350 m^2 s^{-2}, which is more than adequate for tornado development (e.g., Davies-Jones et al. 1990).

The overall atmospheric conditions indicated by the SCP and LSCP paint a similar picture. At 2300 UTC, the SCP has increased substantially over much of Oklahoma with values in southern Oklahoma exceeding 15 in many places (Fig. 5c). The corresponding LSCP has decreased to near zero in many areas except near regions of large LSRH and on the north side of the E complex. In the case of storm complex E, there are multiple storm cells and leftover boundaries from the previous storms that result in non-continuous LSCP values.

6. Short-term forecasts

Assessment of the model environment at 2130 and 2300 UTC indicates regions where left- and right-moving supercells may occur. To determine the capability of the NEWS-e system to forecast splitting supercells, 3-h forecasts of reflectivity and UH were calculated for the first 18 ensemble members beginning at 2130 UTC, followed by 90-min forecasts beginning at 2300 UTC. Figure 7a shows the probability of simulated composite reflectivity >40 dBZ for the 3-h forecast period beginning at 2130 UTC. In northern Oklahoma and southern Kansas, several northeastward-moving reflectivity swaths are present associated with storm complexes C and D. At least one north-northeast swath

Table 2. Severe weather parameters at 2130 or 2300 UTC for selected locations shown in Figs. 3a and 6b.

Time	Label	Lon deg	Lat deg	SBCAPE (J kg^{-1})	SBCIN (J kg^{-1})	3kmSRH (m^2 s^{-2})	3kmLSRH (m^2 s^{-2})	1kmSRH (m^2 s^{-2})	1kmLSRH (m^2 s^{-2})	SCP	LSCP
2130	S1	–98.97	37.07	3445	0	75	–211	38	0	1.2	–3.2
2130	S2	–98.95	35.75	3580	0	109	–165	52	–20	2.2	–2.7
2130	S3	–98.92	34.5	3956	–19	238	–113	143	–3	15.9	–5.3
2300	S4	–98.8	36.5	3592	0	106	–180	98	–14	6.1	–6.7
2300	S5	–98.53	35.1	3236	–51	141	–154	152	0	8.6	–8.1
2300	S6	–97.96	34.76	3281	–26	351	0	354	0	22.3	0

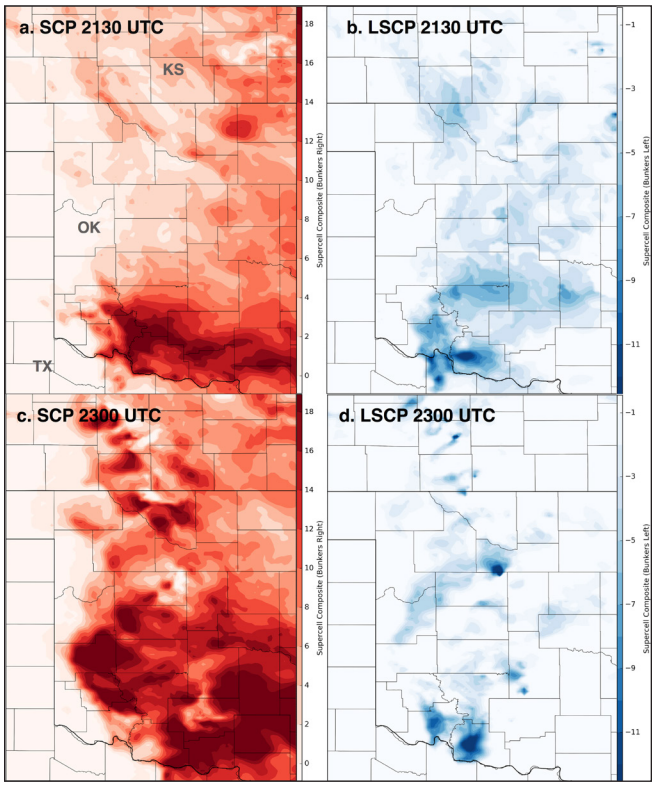

Figure 5. Ensemble mean SCP and LSCP at 2130 UTC (a,b) and 2300 UTC (c,d).

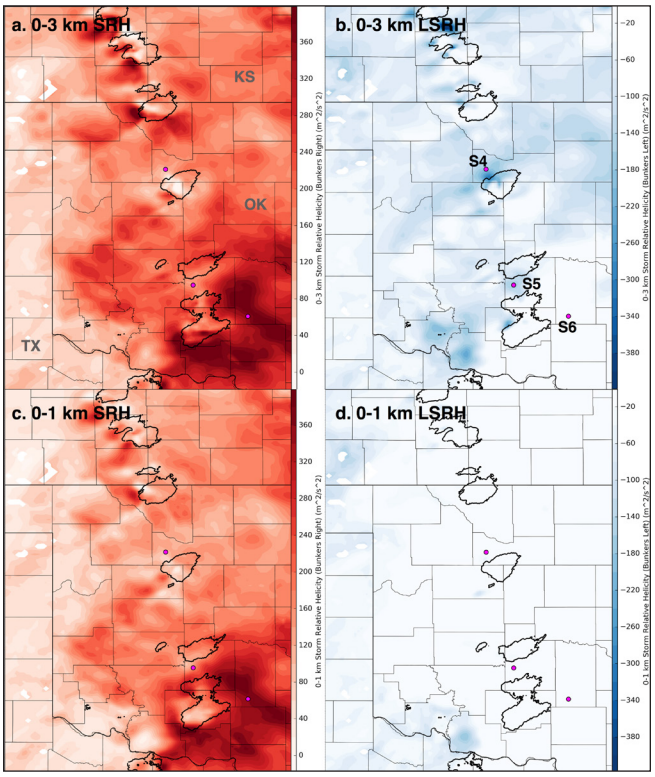

Figure 6. Same as Fig. 3 except for 2300 UTC. Hodograph locations (S4, S5, S6) are denoted by pink dots.

is present that roughly corresponds to C2. Farther south, a lower probability reflectivity swath exists associated with storm complex B with both left- and right-moving supercells evident. In southern Oklahoma, only a short northeastward-moving swath is present with no sign of splitting. To determine the rotational characteristics of these storms, the ensemble mean 2–5-km UH at 5-min intervals for the duration of each forecast is shown in Fig. 7b. The tracks of both cyclonically and anticyclonically rotating supercells are evident in several locations. In northern Oklahoma and southern Kansas, both left- and right-moving supercells are present and roughly corresponding to storm complexes C and D; these persist for the duration of the forecast in this region. Farther south, a single splitting supercell is forecast in central Oklahoma corresponding to complex B, with both left- and right-moving supercells being maintained for the duration of the forecast. In reality, only the left-moving supercell persisted out to 2300 UTC (Fig. 2). In northern Oklahoma, a splitting supercell was forecast to form, but both members dissipated in the model after 45 min. However, the model has yet to analyze any convection at this time, so its ability to develop the correct convective mode on its own is seen as a very positive result.

By 2300 UTC, convection associated with each storm complex except E is now analyzed by the model, with many 90-min reflectivity swaths with >80% probability present (Fig. 7c). In southern Kansas,

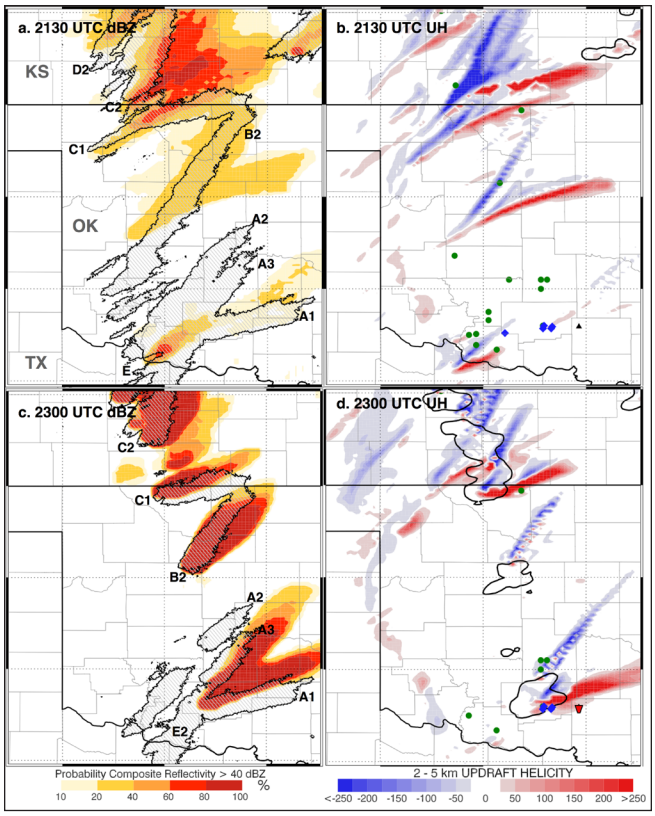

Figure 7. Probability of simulated composite reflectivity >40 dBZ for 3-h forecasts beginning at 2130 UTC (a) and 90-min forecasts beginning at 2300 UTC (c). Black contours in (a) and (c) indicate location of MRMS composite reflectivity >40 dBZ for the duration of the forecast period. Note that the contours for storms A and E overlap each other. Ensemble mean 2–5-km updraft helicity (UH, m^2 s^{-2}) forecasts beginning at 2130 UTC (b) and 2300 UTC (d) with the ensemble mean simulated composite reflectivity >25 dBZ shown at the analysis time. Severe weather reports covering the duration of the forecasts (blue = wind, green = hail, and red = tornado) are shown in panels (b) and (d). Letters denote individual storm complexes as in Fig. 2.

several north-northeastward-moving tracks are present associated with storms C2 and D2. C1 also is evident, but with lower probabilities. Farther south, additional north-northeastward-moving tracks associated with B2 and A3 also are present. Finally, A1 also is analyzed in southern Oklahoma. Both left- and right-moving UH tracks are forecast in northern Oklahoma and southern Kansas corresponding to storm complexes C and D, and negative UH tracks associated with both C2 and D2 also are evident (Fig. 7d). The negative UH track associated with B2 also is well forecast, with the corresponding right-moving supercell now gone from the model forecast. A2 is rather poorly analyzed and has no corresponding negative UH track. Finally, A1 continues to exhibit a well-defined positive UH track that passes near the single tornado report of the event at 0003 UTC 9 May. Finally, no UH tracks were forecast corresponding to storm complex E. This storm was located near the southern boundary of the domain and was poorly initialized throughout the period. By 0000 UTC, left-moving supercells A2, A3, and B2 were all weakening rapidly as they moved into central Oklahoma (Fig. 2f)—where convective inhibition increased. Forecasts tended to extend the UH tracks somewhat past the actual time of dissipation for both left- and right-moving supercells. Overall, the splitting characteristics of the remaining storm complexes were well forecast at both times and were generally consistent with the analyzed atmospheric conditions.

7. Conclusions

Overall, the goal of this study was to determine if the NEWS-e system could produce accurate forecasts of cyclonic and anticyclonic supercells for an event on 8 May 2016 and to determine if the simulated supercells fit within our current scientific understanding of the synoptic and mesoscale environment that produces them. The 8 May 2016 event featured a very clear-cut evolution of long-lived splitting supercells, making it an ideal event for which to conduct this study. Examined alongside modeled hodographs and environmental maps, the model's "choice" in sustaining left- and right-moving supercells could often be explained with various SRH and storm composite parameters for right or left motion similar to those examined in previous studies. In general, right-moving supercells were favored in modeled environments with high right-moving SRH and left-moving supercells in regions of highly negative LSRH.

Probabilistic reflectivity and ensemble mean UH forecasts showed a generally accurate prediction of the occurrence of splitting supercells—even prior to the time that convection had been fully assimilated into the model analysis. Once enough assimilation cycles had occurred so that convection was fully analyzed, the forecast tracks of supercells from reflectivity and UH became much more defined. Analyzing the model's output qualitatively and at a detailed level proved to be an effective way to determine the performance of the NEWS-e system, which is a vital step in the process of verification and understanding strengths,

weaknesses, and biases. For this case, the NEWS-e generated the environment favorable for left- and right-moving supercells, and accurately predicted the location and movement of resulting supercells within that environment.

Acknowledgments. This research was supported by the NOAA National Environmental Satellite, Data, and Information Service as part of the GOES-R program. Partial funding for this research also was provided by the NOAA/Office of Oceanic and Atmospheric Research under NOAA–University of Oklahoma Cooperative Agreement NA11OAR4320072, under the U.S. Department of Commerce. Initial conditions for the NEWS-e system were provided by the Global Systems Division through an experimental HRRR ensemble run during the 2016 Spring Experiment. The NEWS-e design was developed and refined by the NSSL Warn-on-Forecast group in Norman, Oklahoma, and tested during the 2016 Hazardous Weather Testbed. Finally, satellite CWP retrievals were provided in real-time by the NASA Langley Research Center.

REFERENCES

Anderson, J. L, and N. Collins, 2007: Scalable implementations of ensemble filter algorithms for data assimilation. *J. Atmos. Oceanic Technol*., **24**, 1452–1463, Crossref.

____, T. Hoar, K. Raeder, H. Liu, N. Collins, R. Torn, and A. Avellano, 2009: The Data Assimilation Research Testbed: A community facility. *Bull. Amer. Meteor. Soc*., **90**, 1283–1296, Crossref.

Benjamin, S. G., and Coauthors, 2016: A North American hourly assimilation and model forecast cycle: The Rapid Refresh. *Mon. Wea. Rev*., **144**, 1669–1694, Crossref.

Brooks, H. E., C. A. Doswell III, and J. Cooper, 1994: On the environments of tornadic and nontornadic mesocyclones. *Wea. Forecasting*, **9**, 606–618, Crossref.

Brown, R. A., and R. J. Meitín, 1994: Evolution and morphology of two splitting thunderstorms with dominant left-moving members. *Mon. Wea. Rev*., **122**, 2052–2067, Crossref.

Bunkers, M. J., 2002: Vertical wind shear associated with left-moving supercells. *Wea. Forecasting*, **17**, 845–855, Crossref.

____, B. A. Klimowski, J. W. Zeitler, R. L. Thompson, and M. L. Weisman, 2000: Predicting supercell motion using a new hodograph technique. *Wea. Forecasting*, **15**, 61–79, Crossref.

Davies-Jones, R., 1985: Dynamical interaction between an isolated convective cell and a veering environmental wind. Preprints, *14th Conf. on Severe Local Storms*, Indianapolis, IN, Amer. Meteor. Soc., 216–219.

____, D. Burgess, and M. Foster, 1990: Test of helicity as a tornado forecast parameter. Preprints, *16th Conf. on Severe Local Storms*, Kananaskis Park, AB, Canada, Amer. Meteor. Soc., 588–592.

Dostalek, J. F., J. F. Weaver, and G. L. Phillips, 2004: Aspects of a tornadic left-moving thunderstorm on 25 May 1999. *Wea. Forecasting*, **19**, 614–626, Crossref.

Edwards, R., and S. J. Hodanish, 2006: Photographic documentation and environmental analysis of an intense, anticyclonic supercell on the Colorado plains. *Mon. Wea. Rev*., **134**, 3753–3763, Crossref.

____, R. L. Thompson, and C. M. Mead, 2004: Assessment of anticyclonic supercell environments using close proximity soundings from the RUC model. Preprints, *22nd Conf. on Severe Local Storms*, Hyannis, MA, Amer. Meteor. Soc., P1.2. [Available online at ams.confex.com/ams/pdfpapers/81328.pdf.]

Grasso, L. D., and E. R. Hilgendorf, 2001: Observations of a severe left moving thunderstorm. *Wea. Forecasting*, **16**, 500–511, Crossref.

Jirak, I. L., and Coauthors, 2014: An overview of the 2014 NOAA Hazardous Weather Testbed Spring Forecasting Experiment. Preprints, *27th Conf. on Severe Local Storms*, Madison, WI, Amer. Meteor. Soc., 46. [Available online at ams.confex.com/ams/27SLS/webprogram/Manuscript/Paper254650/SLS2014_SFE2014_Overview_Ext_Abstract_Final.pdf.]

Jones, T. A, D. Stensrud, L. Wicker, P. Minnis, and R. Palikonda, 2015: Simultaneous radar and satellite data storm-scale assimilation using an ensemble Kalman filter approach for 24 May 2011. *Mon. Wea. Rev*., **143**, 165–194, Crossref.

____, K. Knopfmeier, D. Wheatley, G. Creager, P. Minnis, and R. Palikonda, 2016: Storm-scale data assimilation and ensemble forecasting with the NSSL Experimental Warn-on-Forecast system. Part II: Combined radar and satellite data experiments. *Wea. Forecasting*, **31**, 297–327, Crossref.

Kain, J. S., and Coauthors, 2008: Some practical considerations regarding horizontal resolution in the first generation of operational convection-allowing NWP. *Wea. Forecasting*, **23**, 931–952, Crossref.

Klemp, J. B., and R. B. Wilhelmson, 1978: Simulations of right- and left-moving storms produced through storm splitting. *J. Atmos. Sci*., **35**, 1097–1110, Crossref.

Monteverdi, J. P., W. Blier, G. Stumpf, W. Pi, and K. Anderson, 2001: First WSR-88D documentation of an anticyclonic supercell with anticyclonic tornadoes: The Sunnyvale–Los Altos, California, tornadoes of 4 May 1998. *Mon. Wea. Rev.*, **129**, 2805–2814, Crossref.

Skamarock, W. C., and Coauthors, 2008: A Description of the Advanced Research WRF Version 3. NCAR Tech. Note NCAR/TN-475+STR, 125 pp, Crossref.

Smith, B. T., R. L. Thompson, J. S. Grams, C. Broyles, and H. E. Brooks, 2012: Convective modes for significant severe thunderstorms in the contiguous United States. Part I: Storm classification and climatology. *Wea. Forecasting*, **27**, 1114–1135, Crossref.

Stensrud, D. J., J.-W. Bao, and T. T. Warner, 2000: Using initial condition and model physics perturbations in short-range ensemble simulations of mesoscale convective systems. *Mon. Wea. Rev*., **128**, 2077–2107, Crossref.

____, and Coauthors, 2009: Convective-scale Warn-on-Forecast system: A vision for 2020. *Bull. Amer. Meteor. Soc*., **90**, 1487– 1499, Crossref.

____, and Coauthors, 2013: Progress and challenges with Warn-on-Forecast. *Atmos. Res*., **123**, 2–16, Crossref.

Thompson, G., R. M. Rasmussen, and K. Manning, 2004a: Explicit forecasts of winter precipitation using an improved bulk microphysics scheme. Part I: Description and sensitivity analysis. *Mon. Wea. Rev*., **132**, 519–542, Crossref.

____, P. R. Field, R. M. Rasmussen, and W. D. Hall, 2008: Explicit forecasts of winter precipitation using an improved bulk microphysics scheme. Part II: Implementation of a new snow parameterization. *Mon. Wea. Rev*., **136**, 5095–5115, Crossref.

Thompson, R. L., R. Edwards, J. A. Hart, K. L. Elmore, and P. Markowski, 2003: Close proximity soundings within supercell environments obtained from the Rapid Update Cycle. *Wea. Forecasting*, **18**, 1243–1261, Crossref.

____, ____, and C. M. Mead, 2004b: An update to the supercell composite and significant tornado parameters. Preprints, *22nd Conf. Severe Local Storms*, Hyannis, MA, Amer. Meteor. Soc., P8.1. [Available online at ams.confex.com/ams/pdfpapers/82100.pdf.]

Wheatley, D. M., K. H. Knopfmeier, T. A. Jones, and G. J. Creager, 2015: Storm-scale data assimilation and ensemble forecasting with the NSSL Experimental Warn-on-Forecast System. Part I: Radar data experiments. *Wea. Forecasting* , **30**, 1795–1817, Crossref.

Wilhelmson, R. B., and J. B. Klemp, 1978: A numerical study of storm splitting that leads to long-lived storms. *J. Atmos. Sci*., **35**, 1974–1986, Crossref.